SoftwareX 7 (2018) 115–121

Contents lists available at ScienceDirect

SoftwareX

journal homepage: www.elsevier.com/locate/softx

Original software publication

Enabling three-dimensional densitometric measurements using laboratory source X-ray micro-computed tomography

M.J. Pankhurst [a,b,c,d,e], R. Fowler [f], L. Courtois [a,b], S. Nonni [a,b], F. Zuddas [g], R.C. Atwood [a], G.R. Davis [h], P.D. Lee [a,b,*]

[a] Research Complex at Harwell, Harwell Campus, OX11 0QX, UK
[b] School of Materials, The University of Manchester, Manchester, M13 9PL, UK
[c] School of Earth and Environment, University of Leeds, Leeds, LS29 9ET, UK
[d] Instituto Technológico y de Energías Renovables (ITER), 38900 Granadilla de Abona, Tenerife, Canary Islands, Spain
[e] Instituto Volcanológico de Canaries (INVOLCAN), 38400 Puerto de la Cruz, Tenerife, Canary Islands, Spain
[f] Scientific Computing Department, Science and Technology Facilities Council, Rutherford Appleton Laboratory, Harwell Campus, OX11 0QX, UK
[g] Instrument Design Division, Science and Technology Facilities Council, Rutherford Appleton Laboratory, Harwell Campus, OX11 0QX, UK
[h] Institute of Dentistry, Queen Mary University of London, London, E1 4NS, UK

ARTICLE INFO

Article history:
Received 11 July 2017
Received in revised form 15 February 2018
Accepted 14 March 2018

Keywords:
Laboratory X-ray micro-computed tomography
Beam characterisation
Python
Beam hardening
Three-dimensional densitometry

ABSTRACT

We present new software allowing significantly improved quantitative mapping of the three-dimensional density distribution of objects using laboratory source polychromatic X-rays via a beam characterisation approach (c.f. filtering or comparison to phantoms). One key advantage is that a precise representation of the specimen material is not required. The method exploits well-established, widely available, non-destructive and increasingly accessible laboratory-source X-ray tomography. Beam characterisation is performed in two stages: (1) projection data are collected through a range of known materials utilising a novel hardware design integrated into the rotation stage; and (2) a Python code optimises a spectral response model of the system. We provide hardware designs for use with a rotation stage able to be tilted, yet the concept is easily adaptable to virtually any laboratory system and sample, and implicitly corrects the image artefact known as beam hardening.

Code metadata

Current code version	*1.0*
Permanent link to code/repository used of this code version	https://github.com/ElsevierSoftwareX/SOFTX-D-17-00053
Legal Code License	*Apache 2.0*
Code versioning system used	*SVN*
Software code languages, tools, and services used	*Python 2.7*
Compilation requirements, operating environments & dependencies	*The main Python modules that users may need to install are numpy, matplotlib, scipy, tifffile*
If available Link to developer documentation/manual	https://ccpforge.cse.rl.ac.uk/svn/tomo_bhc/trunk/doc/
Support email for questions	ronald.fowler@stfc.ac.uk

Software metadata

Current software version	*1.0*
Permanent link to executables of this version	*NA*
Legal Software License	*Apache 2.0*
Computing platforms/Operating Systems	*Linux, Windows, MacOS*
Installation requirements & dependencies	*Python 2.7*
If available, link to user manual — if formally published include a reference to the publication in the reference list	*NA*
Support email for questions	ronald.fowler@stfc.ac.uk

* Corresponding author at: School of Materials, The University of Manchester, Manchester, M13 9PL, UK.
E-mail address: pdlee123@gmail.com (P.D. Lee).

https://doi.org/10.1016/j.softx.2018.03.004

1. Introduction

Three-dimensional (3D) densitometry can be conducted using monochromatic X-ray imaging (synchrotron) and tomographic reconstruction [1,2]. The relationship between attenuation and a homogeneous object's thickness is linear for a single X-ray energy (e.g. [3]). Single energy calculated attenuation is also linear since the detector response, in theory, is constant (see [4] for a discussion of detectors and sources).

Measuring density quantitatively and accurately using a typical laboratory X-ray imaging setup, however, is non-trivial. This is because conventional impact X-ray sources produce polychromatic beams (which can change from scan to scan), and attenuation is strongly dependent on X-ray energy (Fig. 1). Furthermore, conventional detectors do not differentiate energy (only flux) and do not have uniform response over the whole energy range. Finally, there may be no practical way of placing precisely known thicknesses of the exact material of interest into the beam, which would allow an internal calibration between attenuation and thickness to be made (for that material only).

The detected signal is an outcome of the combination of three variables: the incoming spectrum, the sample-specific interaction with that beam, and the response of the detector. Our aim here is to make quantitative densitometry practical, and adaptable to any laboratory setting, by demonstrating a method of characterising the beam spectra that can be easily integrated into day-to-day laboratory procedure. Once the beam is characterised using our code, correction factors for any given material can be calculated with respect to that material's attenuation of a monochromatic beam. With the correction applied to the projection data, the reconstructed tomograms are a quantitative and reproducible measure of that objects' density, and with beam-hardening minimised.

2. Background

In theory, if the proportions of different energies and the composition of the specimen are known, a good estimate of density can be derived from the reconstructed X-ray image. All that is required in order to calculate the attenuation and thus density of the object the beam passes through is knowledge of the X-ray spectra used, and the response function of the detector. The non-linearity in the response due to polychromatic X-rays can then be corrected to a linear relationship between response and sample thickness.

X-ray spectra can be calculated, which gives a good approximation for the energies emitted from polychromatic X-ray sources. Yet these values are not precisely known for real X-ray tubes and there are a number of other uncertainties, such as the efficiency of the detectors, which influence the signal recorded. Today's industrial X-ray radiography and tomography equipment does not attempt to apply corrections based on calculations from measurements made from the beam itself. Instead, the density phantoms suitable for some purposes are provided and are used as calibration standards to apply to images ([5]; see also method notes in [6]). Qualitative correction routines that improve the visual appearance of the result – but do not provide an estimate of the true absorption properties – are also provided by scanner manufacturers. While the artefacts appearing in such images may be neglected for some purposes, these can at best complicate the analysis and at worst lead to spurious results.

During a tomography acquisition, the average X-ray path lengths common to a single voxel are shorter when that voxel is near the edge of the object (Fig. 2a). This causes 'beam hardening' to manifest as image cupping in tomographic reconstructions based upon linear absorption. The artefact manifests as relative brightening at the edges of reconstructed objects and darkening in the middle (Fig. 2b). Without correction of the original projection data (i.e. the response per pixel) this artefact precludes accurate densitometry. For objects that actually have a radial distribution of density such as a tooth or a bone, or chemically zoned crystals, the beam hardening effect becomes confounded with the very property the experiment is intended to measure (see Fig. 3).

Understanding and overcoming image artefacts inherent to the polychromatic nature of laboratory-source X-ray spectra is thus a vital task (e.g. [7]). This is because the greyscale value assigned to a reconstructed voxel is routinely used to digitally map an object's features, in order to extract textural [8] and chemical information [9]. Applications that rely on high confidence when using the greyscale value as a key image parameter range from geological and environmental [10–13] to biomedical [14], to transport and energy [15] and material engineering applications [16]. Due to this numerical 'smearing', however, beam hardening artefacts have long posed a major limitation to quantitative 3D image analysis.

3. Our approach

In this contribution, we report an advance in the development of a method of three-dimensional densitometric measurement by characterising the polychromatic beam and the detector response [17–21]. First, the scan settings are decided upon, and then that beam is characterised. The beam is used to take projection data through different thicknesses of materials of known attenuation (that bracket that of the object). The images provide raw intensity data that can be then compared to a modelled system [17]. Since the model is not exact, it is necessary to adjust some of the parameters to obtain an optimal fit to the measured data.

Measurements are conducted using a nonlinear optimisation process to obtain a function that represents the X-ray energy response of the system [17]. Where the specimen material composition is known, the function can be used to generate a calibration curve for that material using published X-ray attenuation values, for instance see [22]. This approach produces a curve approximating the real, non-linear relationship between total polychromatic beam attenuation and the expected attenuation with monochromatic radiation [20] which may be easily and simply applied in existing tomography equipment.

A current limitation of this algorithm is that the resulting correction curve is specific to a single phase. If, for example, the material of interest is encapsulated or held in place by resin, or surrounded by soft tissue etc., the presence of this second phase will decrease the accuracy of our approach. In cases where one phase contributes little to the attenuation, the method still gives an accurate estimate of the dominant phase. Similarly, for multi-phase specimens where there is a macroscopically uniform distribution of the phases, the method gives good overall beam-hardening correction that can improve the segmentation of the individual phases. An enhanced version of this method for more accurate densitometric measurement in dual phase systems is under development [23].

Our approach is distinct from filtration, which works to remove low energy X-rays from the beam, thereby narrowing the window of beam energy used toward an ideal case (see first paragraph). Since the ideal case is not possible in the laboratory (even if a single energy was achieved the flux would be too low for imaging in any practical scenario), filtration serves to reduce the effects of beam hardening, but does not provide quantitative densitometry.

4. Method developments

4.1. Hardware

It has long been common practice to use a step wedge of aluminium as an attenuation standard (e.g. [24]). Aluminium is

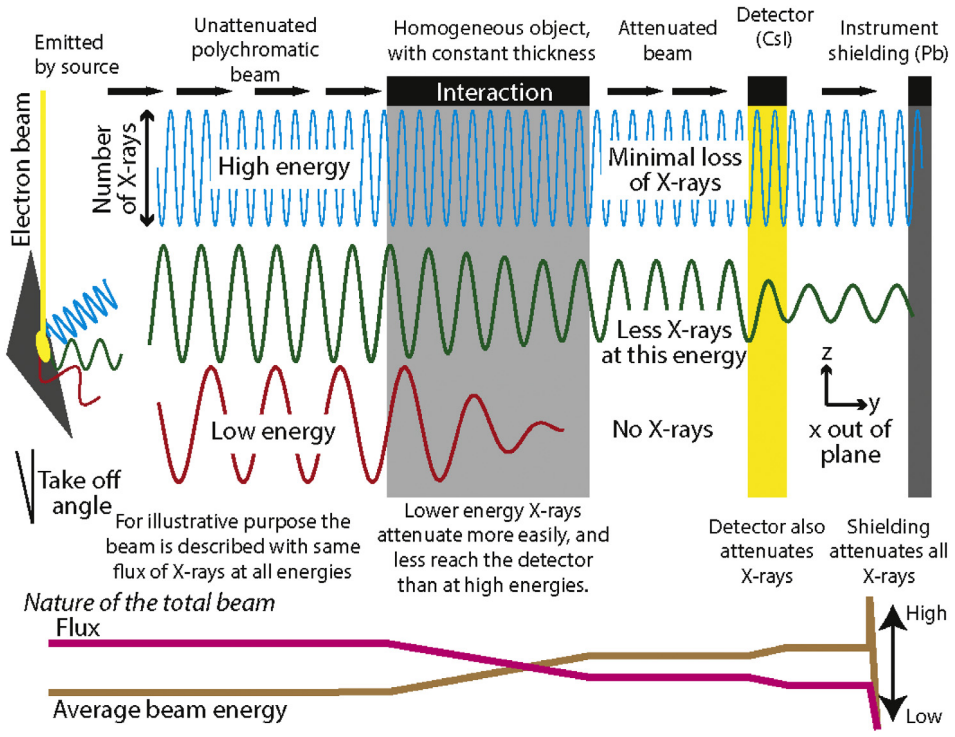

(a) X-ray path in a typical laboratory scanner.

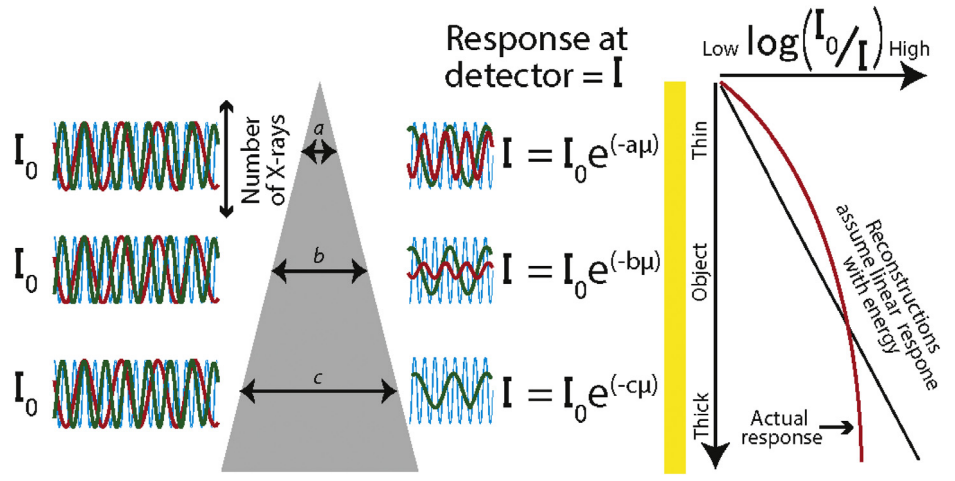

(b) Effect of 2D thickness.

Fig. 1. Schematic describing the physical cause of beam-hardening in tomographic image reconstructions from a polychromatic X-ray source. (a) X-rays of different energies are generated by excitation of a source (usually W metal) using a focussed electron beam. Lower energy X-rays attenuate more easily and as such fewer reach the detector relative to higher energies, for a given thickness of material. (b) The attenuation at all energies is proportional to object thickness, and thus the combined effect described in (a) and (b) is that the response at the detector (I) is disproportionately lower from ray paths that interact over long distances through an object, compared to those that interact over a short distance.

easy to work with and available in high purity. The step wedge is practical; projection data through known thicknesses are obtained either simultaneously, or by simply moving different thicknesses of the step wedge into the field of view.

Using a single material is simple and self-consistent, yet the use of a number of different materials provides a more complete, and thus better constrained, characterisation of the beam [18,21]. The use of multiple elements is also practical; if the attenuator was all aluminium, some parts would need to be several cm at high energies. If they were all copper, some parts would need to be a few μm thick at low energies. A simple design that incorporated numerous materials was built by Evershed [25], allowing the insertion of a variety of materials between the source and the detector.

In Fig. 4 we show a new development; a 'crown' of materials set into individual pegs arranged around the outside of a single circular base plate. This geometry allows us to load the crown with many materials, in this case 18. Full design drawings can be found in the supplementary material. It should be noted that this specific design is our preferred option here, because our stage can be tilted. For systems that do not have a tilt option on the rotation stage, the carousel solution of Davis et al. [20] can be used instead. If permanent mounting is not possible (i.e. integrated with the stage) it can be scanned separately as if it were a specimen.

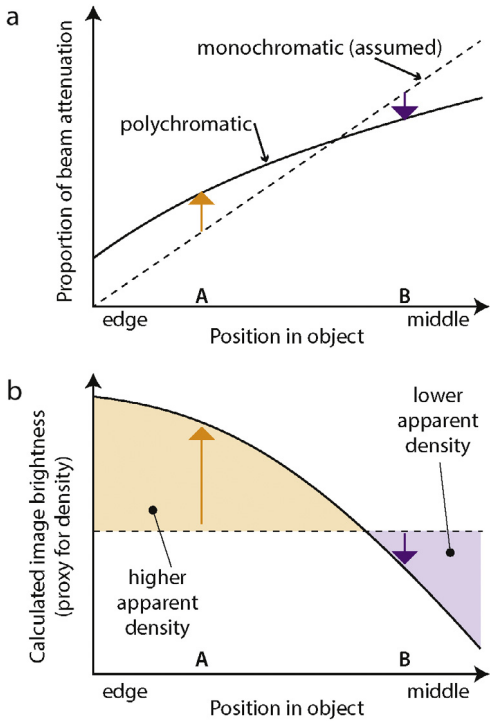

Fig. 2. Schematic explanation of beam hardening. (a) With increasing thickness, proportionately fewer X-rays are transmitted through an object. The relationship is linear for monochromatic beams. When using polychromatic beams, the low energy X-rays are attenuated more strongly than the higher energy X-rays, and are disproportionately removed by comparatively thin interaction lengths. Thus at position A, more signal is detected than if a monochromatic beam was used; position B results in less signal. (b) Since reconstructions assume a linear response, the observed signal is calculated as higher than real density (recorded as image brightness) at position A, and lower at position B.

Table 1
Materials used to acquire projection data. Note: thicknesses were measured with electronic callipers.

Position	Material	Thickness (mm)	2σ ($n = 4$)
1	Copper	1.992	0.015
2	Aluminium	0.051	0.002
3	Aluminium	0.097	0.001
4	Aluminium	0.255	0.003
5	Aluminium	0.509	0.006
6	Aluminium	0.999	0.002
7	Aluminium	2.0	0.007
8	Aluminium	3.0	0.007

4.2. Software

The Python code significantly expands upon, and simplifies, an Interactive Data Language (IDL) script that was first written during the formulation of the original concept [17]. The code can be obtained via the web at https://ccpforge.cse.rl.ac.uk/svn/tomo_bhc/trunk/, along with a user guide. We have taken this opportunity to produce a correction factor as a 4th order polynomial, which is more suitable for a wide range of instruments to employ (i.e. a custom 4th order polynomial can be used in standard *Nikon X-Tek* software). A high-level workflow of the method is illustrated in Fig. 5. See also supplementary data for detailed code description, including validation against the IDL script. The code's functions are computationally basic; curve fitting and simple modelling of X-ray attenuation.

4.3. Application to a number of materials

We have conducted a number of scans and corrections that demonstrate the software's applicability across fields of research ranging from aerospace components (e.g. [26]), to geological (e.g. [27]) and biomedical applications (e.g. [28]), and for different imaging purposes. The first cases selected were light alloy components, as tomography is routinely used for defect detection [29,30]) and for designing new compositions [31,32]. Furthermore, typifying such alloys using laboratory source X-rays for use as random absorption masks in phase scattering imaging is an emerging application [33]. A block of high purity aluminium and a block of Al–Cu alloy (15% Cu; see [34,35] for details) were scanned using the same equipment described above, set at a nominal maximum energy of 70 kV, taking 3154 projections around 360° and using a 1.0 mm Al filter. We used the calibrated modelling approach to correct these projections to those expected of a 40 kV monochromatic beam using a calibration curve generated for Al, and Al–15%Cu, respectively. A chicken wing bone (dry) was scanned at a nominal maximum of 35 kV with no pre-filtration of the polychromatic beam, as a key application is biomedical [36] and determining the efficacy of biomaterials in implants [14,37].

5. Results

Fig. 6 shows typical results from these materials ranging from physical to life sciences applications, and illustrates potential applications and some limitations. The method accurately determines the linear attenuation coefficient of high purity aluminium in three-dimensions with little to no discernible beam hardening artefacts (Fig. 6ai), within approximately 1% precision (Fig. 6aii). Noise would be further lessened using additional frames per projection. The results are a significant improvement over uncorrected or automated proprietary beam-hardening corrections.

When applied to a heterogeneous material comprised of two phases with different densities, such as an Al–Cu alloy (Fig. 6b), the method can correct for beam hardening using the bulk composition. However, retrieving accurate densitometric measurements on a per-voxel basis is non-trivial. This is due to the correction being applied assuming a perfectly mixed material, whereas the alloy is composed of dendritic crystals of Al and Cu at a fine scale (Fig. 6bi, ii). Although the method removes the bulk beam hardening (Fig. 6biii) and provides a reproducible image intensity for each of the phases, there is an additional uncertainty as compared to a single phase material when calculating density on the basis of measured linear attenuation co-efficient per voxel. The use of *in situ* calibration samples would overcome this limitation, allowing normalisation of the now regularised image. Since the imaging is made reproducible when beam calibrations are performed, calibration would only need to be performed once, and the calibrations could be used throughout large-scale tomography campaigns.

Finally, we chose the bone as a life sciences example in which the hardening artefact is confounded with the real density variation (Fig. 6c). Bone is a material that is also comprised of two phases, and exhibits a radially distributed density distribution. Beam hardening accentuates the bias toward higher intensity voxels at the edges of the chicken bone (Fig. 6ci) as well-illustrated by the uncorrected profile (Fig. 6cii). In these circumstances it may be tempting to use beam hardening corrections within propriety software to arrive at an image wherein the peaks are of equal height, yet this would risk overcorrecting and blurring the image.

Since the soft tissue has low attenuation (and thus is influenced by beam hardening less so than hard tissue), we corrected using a calibration curve generated for bone alone. In the corrected image and profile, the density distribution still exhibits significant increase with distance from the centre, but this is a genuine characteristic of bone. Our method has not spuriously removed this variation as would happen with the methods described above.

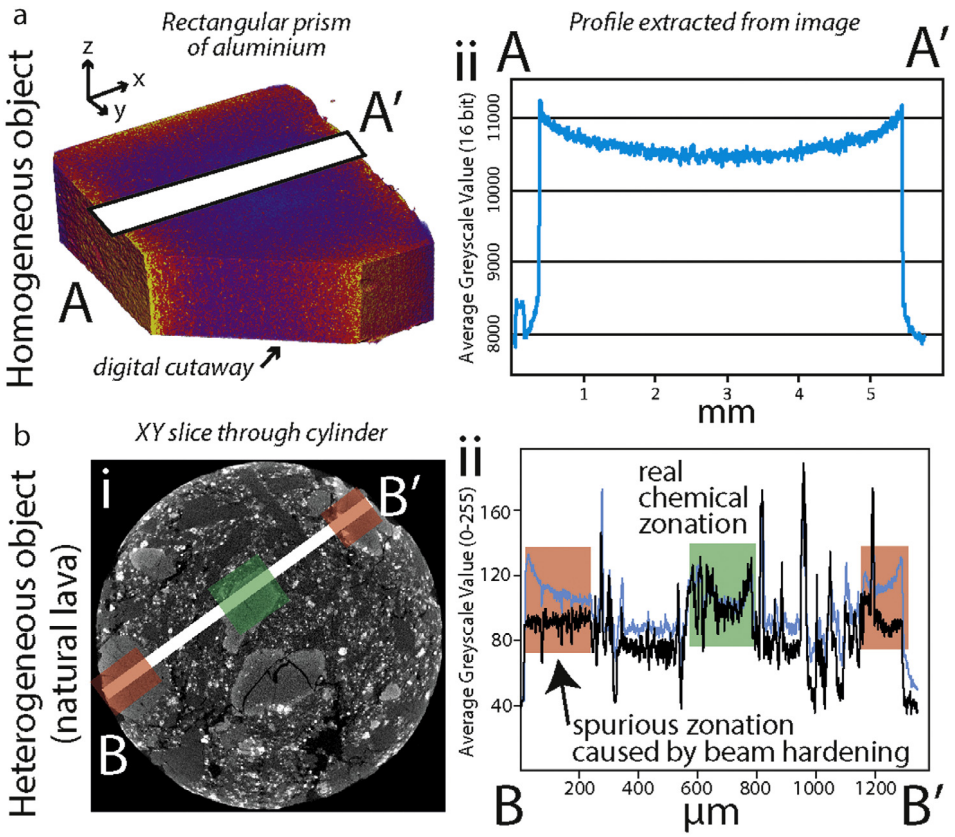

Fig. 3. Example of beam hardening artefacts in (a) a homogeneous object; aluminium and (b) heterogeneous object; natural lava exhibiting a number of crystal phases with different densities. Cupping is illustrated by an *X* direction profile across the aluminium block (aii), whereas the influence is cryptic in the lava (bi), yet can be observed to imparts errors when relating chemical zonation to differences in image brightness (bii).

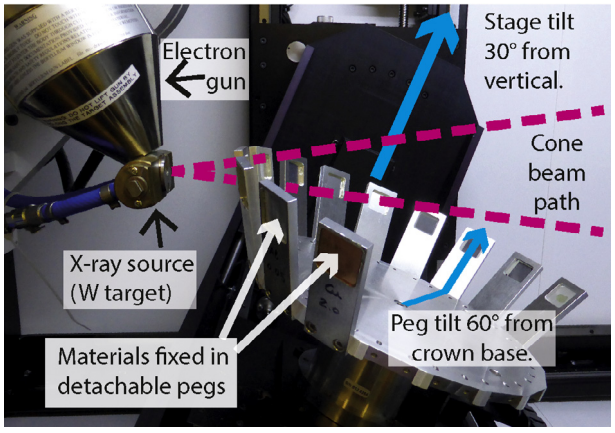

Fig. 4. Crown mounted within a typical laboratory XMT scanner. For collection of projections the material is within 1 cm of the X-ray target; greater distance is shown for illustrative purposes. For description of the materials see Table 1.

6. Discussion

Many commercially available software packages that are coupled with X-ray tomography systems offer a suite of options to apply pre-reconstruction beam hardening corrections. These are either polynomial equations fit to an assumed background which is then removed via applying a correction factor, or are determined by automated proprietary methods, but these techniques are not material specific. In practice, several of these are usually applied during the reconstruction of a small selection of slices.

The eventual choice of technique to be used for the entire volume is determined by the user or by basic image analysis (e.g. see Fig. 6), by seeking a flat profile across a slice where density is assumed to be constant. Any such approach introduces the potential to 'correct-out' real signal, or over- or under-estimate beam hardening, potentially leading to spurious results and interpretation. Where density is assumed to be homogeneous (on a given scale, i.e. Fig. 6b), and especially where density is likely to not be homogeneous (Fig. 6c) this potential for error is amplified.

If we are to use laboratory XMT as a quantitative and reproducible 3D densitometric tool a more rigorous and reproducible approach is required. Our spectrum and response modelling method characterises the beam at the time of acquisition from a specific sample, which imlicitly allows for variations in the hardware through time. The corrections may be calculated and applied line-by-line, thus, accounting for the relationship between X-ray take-off angle and energy spectrum.

Our methodology addresses issues that are impossible to monitor when traditional non-specific, qualitative, beam hardening corrections are used. For example, anode pitting increases self-absorption in the target material [18], producing changes in the spectrum emitted. In turn, these changes are reflected in the calculated attenuation of a specimen, leading to deviations in apparent density. These changes are immediately incorporated via the carousel/crown calibration. Further, the calibration changes can be monitored to diagnose such problems and trigger maintenance.

Calibration curves and correction factors specific to the sample of interest may be generated using publicly available data (i.e. XCOM). Thus our approach has value for a wide range of research questions. The calibration data can be archived so that any future developments in calibration methods, or reconstruction algorithms, can be applied retrospectively to improve the quality

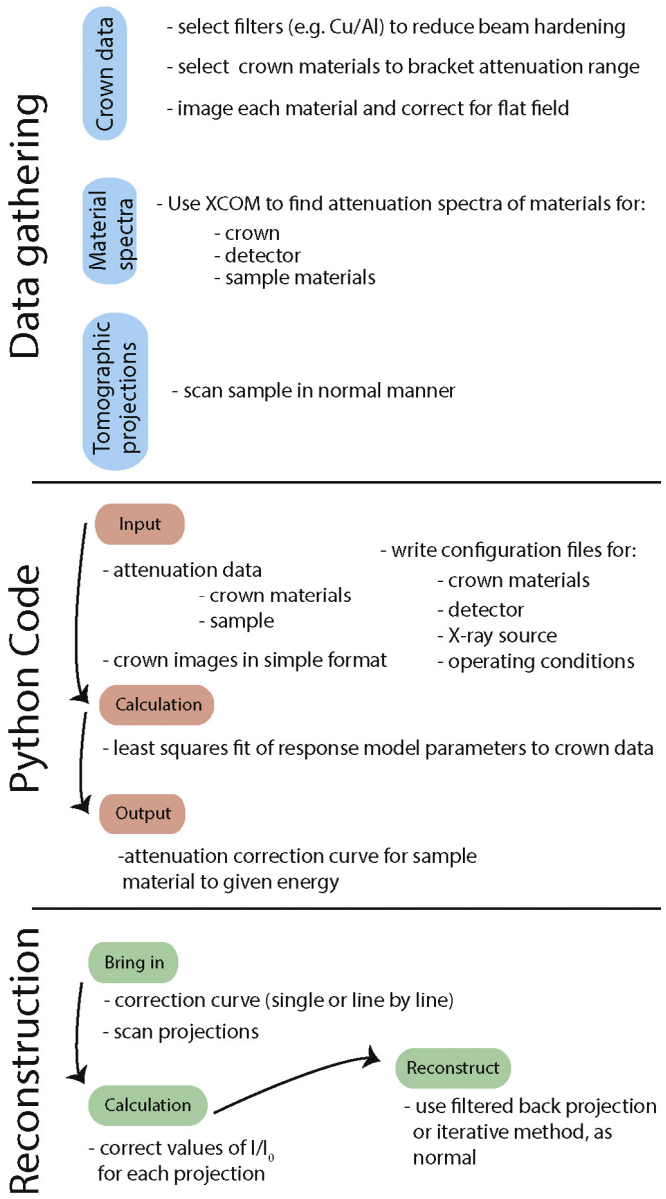

Fig. 5. Flow diagram illustrating steps of the material-specific method to correct beam hardening image artefacts.

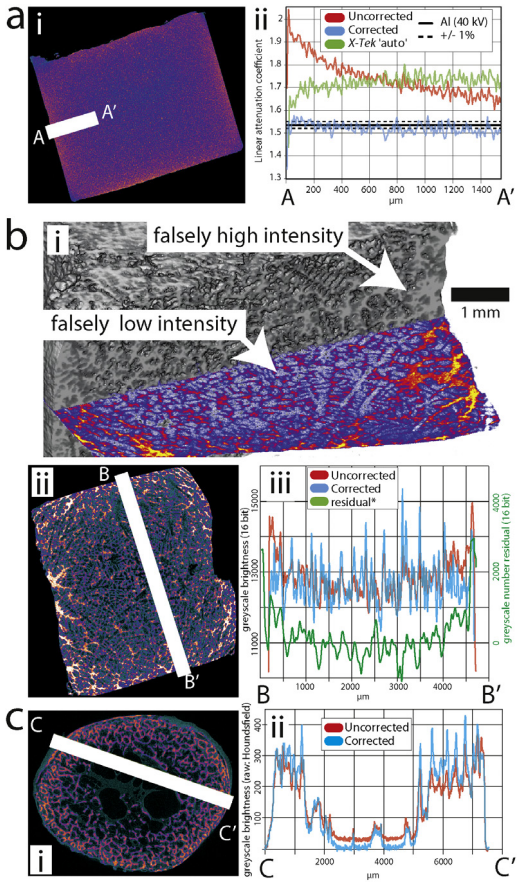

Fig. 6. Illustration of applications and limitations. In all examples the image is the uncorrected; chosen to exhibit features that will be familiar to many readers. (a) Single phase material with homogeneous density distribution on broad and fine scales; high purity aluminium. (b) Two-phase material with homogeneous distribution of heterogeneous texture at fine scales; Al–Cu alloy. *Calculated using a 50 voxel rolling average used as a crude high-pass filter. (c) Two-phase material with heterogeneous density distribution of heterogeneous texture at fine scales and naturally including apparent radial variation of density; chicken wing bone.

of old scans. We recommend any material be used in the crown to acquire the characterisation data, so long as the most attenuating piece of material is more attenuating that the object being scanned, although the method does not break down beyond this range and some extrapolation is acceptable. The thinnest test pieces should be chosen to approximate attenuation through the very edges of the specimen. We also recommend using the approach in combination with some pre-filtering of soft X-rays.

The characterisation methodology is easily adapted to most types of X-ray systems. For instance, custom-bay type scanners could use a roof-mounted stage to hold a crown, while a miniaturised carousel would work for a desktop scanner. The crown design provided is ideal for laboratories that scan a wide variety of objects with different densities and chemical compositions. The large number of available positions lends itself to being easily adapted for a wide range of scan conditions. The software is now available through the Collaborative Computation Project — Imaging (CCPi). Running the code usually takes less than a few minutes on a typical laptop computer.

Acknowledgements

This work was funded by the EPSRC UK (EP/I02249X/1, EP/J010456/1, EP/M009688/1 and EP/M022498/1) and NERC UK (NE/M013561/1, NE/M001458/1, NE/N018575/1). MP gratefully acknowledges the support of an AXA Research Fund Fellowship. Biao Cai is thanked for providing the alloy sample.

Appendix A. Supplementary data

Supplementary material related to this article can be found online at https://doi.org/10.1016/j.softx.2018.03.004.

References

[1] Cloetens P, Bolle E, Ludwig W, Baruchel J, Schlenke M. Absorption and phase imaging with synchrotron radiation. Europhys News 2001;32(2):46–50.
[2] Herman GT. Fundamentals of computerized tomography: Image reconstruction from projections. Springer Science & Business Media; 2009.
[3] McCullough EC. Photon attenuation in computed tomography. Med Phys 1975;2(6):307–20.
[4] Shefer E, Altman A, Behling R, Goshen R, Gregorian L, Roterman Y, Uman I, Wainer N, Yagil Y, Zarchin O. State of the art of CT detectors and sources: a literature review. Curr Radiol Rep 2013;1(1):76–91.
[5] Bouxsein ML, Boyd SK, Christiansen BA, Guldberg RE, Jepsen KJ, Müller R. Guidelines for assessment of bone microstructure in rodents using micro–computed tomography. J Bone Miner Res 2010;25(7):1468–86.

[6] Bruker . Density measurement by MicroCT, Vol. 1. Bruker Micro-CT Academy; 2014.
[7] Ketcham RA, Carlson WD. Acquisition, optimization and interpretation of X-ray computed tomographic imagery: Applications to the geosciences. Comput Geosci 2001;27(4):381–400.
[8] Liu Y, Kiss AM, Larsson DH, Yang F, Pianetta P. To get the most out of high resolution X-ray tomography: A review of the post-reconstruction analysis. Spectrochim Acta B 2016;117:29–41.
[9] Pankhurst MJ, Dobson KJ, Morgan DJ, Loughlin SC, Thordarson T, Courtios L, Lee PD. Directly monitoring the magmas fuelling volcanic eruptions in near-real-time using X-ray micro-computed tomography. J Petrol 2014;55(3):671–84.
[10] Archilha NL, Missagia RM, Hollis C, De Ceia MAR, McDonald SA, Lima Neto IA, Eastwood DS, Lee P. Permeability and acoustic velocity controlling factors determined from x-ray tomography images of carbonate rocks. AAPG Bull 2016;100(8):1289–309.
[11] Lin Q, Barker D, Dobson K, Lee P, Neethling S. Modelling particle scale leach kinetics based on X-ray computed micro-tomography images. Hydrometallurgy 2016;162:25–36.
[12] Lin Q, Neethling S, Dobson KJ, Courtois L, Lee PD. Quantifying and minimising systematic and random errors in X-ray micro-tomography based volume measurements. Comput Geosci 2015;77:1–7.
[13] Reyes-Dávila GA, Arámbula-Mendoza R, Espinasa-Pereña R, Pankhurst MJ, Navarro-Ochoa C, Savov I, Vargas-Bracamontes DM, Cortés-Cortés A, Gutiérrez-Martínez C, Valdés-González C, Domínguez-Reyes T, González-Amezcua M, Martínez-Fierros A, Ramírez-Vázquez CA, Cárdenas-González L, Castañeda Bastida E, Vázquez Espinoza de los Monteros DM, Nieto-Torres A, Campion R, Courtois L, Lee PD. Volcán de Colima dome collapse of July, 2015 and associated pyroclastic density currents. J Volcanol Geotherm Res 2016;320:100–6.
[14] Geng H, Todd NM, Devlin-Mullin A, Poologasundarampillai G, Kim TB, Madi K, Cartmell S, Mitchell CA, Jones JR, Lee PD. A correlative imaging based methodology for accurate quantitative assessment of bone formation in additive manufactured implants. J Mater Sci: Mater Med 2016;27(6).
[15] Yufit V, Shearing P, Hamilton RW, Lee PD, Wu M, Brandon NP. Investigation of lithium-ion polymer battery cell failure using X-ray computed tomography. Electrochem Commun 2011;13(6):608–10.
[16] Withers PJ, Preuss M. Fatigue and damage in structural materials studied by X-ray tomography. Annu Rev Mater Res 2012;42:81–103.
[17] Davis G, Jain N, Elliott J. A modelling approach to beam hardening correction. In: Proceedings optical engineering+ applications. International Society for Optics and Photonics; 2008. p. 70781E-70781E-70710.
[18] Davis GR, Evershed AN, Mills D. Recent developments in the MuCAT microtomography facility. In: Proceedings SPIE optical engineering+ applications. International Society for Optics and Photonics; 2012. p. 85060E-85060E-85067.
[19] Davis GR, Evershed AN, Mills D. Quantitative high contrast X-ray microtomography for dental research. J Dent 2013;41(5):475–82.
[20] Davis GR, Evershed ANZ, Mills D. Characterisation of materials: Determining density using X-ray microtomography. Mater Sci Technol 2015;31(2):162–6.
[21] Evershed AN, Mills D, Davis G. Multi-species beam hardening calibration device for x-ray microtomography. In: Proceedings SPIE optical engineering+ applications. International Society for Optics and Photonics; 2012. p. 85061N-85061N-85012.
[22] Berger MJ, Hubbell J, Seltzer S, Chang J, Coursey J, Sukumar R, Zucker D, Olsen K. XCOM: photon cross sections database. In: NIST standard reference database, vol. 8; 2016. p. 3587–97.
[23] Davis G, Mills D. 2D beam hardening correction for micro-CT of immersed hard tissue, vol. 9967; 2016. 996707-996707-996708.
[24] Luboshez B. On measuring and expressing X-ray quality in radiography. Br J Radiol: BIR Sect 1925;30(296):81–9.
[25] Evershed ANZ. Multi-material approach to beam hardening correction and calibration in X-ray microtomography [Ph.D.], University of London; 2013. p. 207.
[26] Sloof WG, Pei R, McDonald SA, Fife JL, Shen L, Boatemaa L, Farle A-S, Yan K, Zhang X, van der Zwaag S, Lee PD, Withers PJ. Repeated crack healing in MAX-phase ceramics revealed by 4D in situ synchrotron X-ray tomographic microscopy. Sci Rep 2016;6:23040.
[27] Figueroa Pilz F, Dowey PJ, Fauchille A-L, Courtois L, Bay B, Ma L, Taylor KG, Mecklenburgh J, Lee PD. Synchrotron tomographic quantification of strain and fracture during simulated thermal maturation of an organic-rich shale, UK Kimmeridge Clay. J Geophys Res: Solid Earth 2017;122(4):2553–64.
[28] Yue S, Lee PD, Poologasundarampillai G, Yao Z, Rockett P, Devlin AH, Mitchell CA, Konerding MA, Jones JR. Synchrotron X-ray microtomography for assessment of bone tissue scaffolds. J Mater Sci: Mater Med 2010;21(3):847–53.
[29] Karagadde S, Lee PD, Cai B, Fife JL, Azeem MA, Kareh KM, Puncreobutr C, Tsivoulas D, Connolley T, Atwood RC. Transgranular liquation cracking of grains in the semi-solid state. Nature Commun 2015;6:8300.
[30] Kareh KM, Lee PD, Atwood RC, Connolley T, Gourlay CM. Revealing the micromechanisms behind semi-solid metal deformation with time-resolved X-ray tomography. Nature Commun 2014;5:4464.
[31] Connell LS, Romer F, Suarez M, Valliant EM, Zhang Z, Lee PD, Smith ME, Hanna JV, Jones JR. Chemical characterisation and fabrication of chitosan-silica hybrid scaffolds with 3-glycidoxypropyl trimethoxysilane. J Mater Chem B 2014;2(6):668–80.
[32] Puncreobutr C, Phillion A, Fife J, Lee P. Coupling in situ synchrotron X-ray tomographic microscopy and numerical simulation to quantify the influence of intermetallic formation on permeability in aluminium–silicon–copper alloys. Acta Mater 2014;64:316–25.
[33] Hongchang Wang, Biao Cai, Matthew James Pankhurst, Tunhe Zhou, Yogesh Kashyap, Robert Atwood, Nolwenn Le Gall, Peter Lee, Michael Drakopoulos, Kawal Sawhney. X-ray phase contrast imaging with engineered porous materials over 50 keV. J Synchrotron Radiat [in press].
[34] Cai B, Lee PD, Karagadde S, Marrow TJ, Connolley T. Time-resolved synchrotron tomographic quantification of deformation during indentation of an equiaxed semi-solid granular alloy. Acta Mater 2016;105:338–46.
[35] Cai B, Wang J, Kao A, Pericleous K, Phillion AB, Atwood RC, Lee PD. 4D synchrotron X-ray tomographic quantification of the transition from cellular to dendrite growth during directional solidification. Acta Mater 2016;117:160–9.
[36] Staines KA, Madi K, Mirczuk SM, Parker S, Burleigh A, Poulet B, Hopkinson M, Bodey AJ, Fowkes RC, Farquharson C, Lee PD, Pitsillides AA. Endochondral growth defect and deployment of transient chondrocyte behaviors underlie osteoarthritis onset in a natural murine model. Arthritis Rheum 2016;68(4):880–91.
[37] Atwood R, Jones J, Lee P, Hench L. Analysis of pore interconnectivity in bioactive glass foams using X-ray microtomography. Scr Mater 2004;51(11):1029–33.